JCTC Journal of Chemical Theory and Computation

Article

pubs.acs.org/JCTC

Multireference Ab Initio Density Matrix Renormalization Group (DMRG)-CASSCF and DMRG-CASPT2 Study on the Photochromic Ring Opening of Spiropyran

Fengyi Liu,[†] Yuki Kurashige,[‡] Takeshi Yanai,[‡] and Keiji Morokuma*,[†]

[†]Fukui Institute for Fundamental Chemistry, Kyoto University, Kyoto 606-8103, Japan

[‡]Institute for Molecular Science, 38 Nishigo-Naka, Myodaiji, Okazaki 444-8585, Japan

Supporting Information

ABSTRACT: The photochromic ring-opening reaction of spiropyran has been revisited at the multireference CASSCF and CASPT2 level with a CAS(22e,20o) active space, in combination with density matrix renormalization group (DMRG) methods. The accuracy of the DMRG-CASSCF and DMRG-CASPT2 calculations, with respect to the number of renormalized states, the number of roots in state-averaged wave functions, and the number basis functions, was examined. For the current system, chemically accurate results can be obtained with a relatively small number of renormalized states. The nature and vertical excitation energies of the excited (S_1 and S_2) states are consistent with conventional CAS(or RAS)PT2 with medium active spaces. The capability of the DMRG-CASSCF method in the optimization of molecular geometry is demonstrated for the first time. The computation costs (several hours per optimization cycle) are comparable with that of the conventional CASSCF geometry optimization with small active space. Finally, the DMRG-PT2 computed S_1-MEP for the C−O and C−N bond-cleavage processes show good agreement with our previous calculations with a CAS(12e,10o) active space [Liu, F.; Morokuma, K. *J. Am. Chem. Soc.* **2013**, *135*, 10693−10702]. Especially, the role of the HOOP valleys in the $S_1 \rightarrow S_0$ nonadiabatic decay has been confirmed.

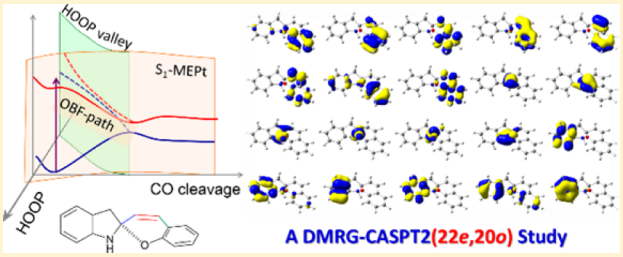

1. INTRODUCTION

Theoretical treatment of photochemical reactions involving excited electronic states has been a challenging problem for a long time. Describing an excited state usually requires a multireference wave function (WF), such as that provided by the complete active space self-consistent field (CASSCF) method.[1] In a CASSCF algorithm, electronic (static) correlation inside the active space is evaluated at the full configuration interaction (FCI) level, while the remaining electron (dynamic) correlation can be treated, on top of the CASSCF WF, using multireference dynamical electron-correlation approaches such as second-order perturbation (PT2) methods. Although this combination is well-established and widely used in solving many multireference problems, there remains a critical drawback. The number of configurations in CASSCF WF exhibits an exponential dependence on the size of the active space. Correspondingly the computation costs, in most cases, restrict the application of the method to small- and medium-sized molecules.

The recently developed multireference Density Matrix Renormalization Group (DMRG) method,[2−8] among many other efforts, has emerged as a most promising solution for the aforementioned problem. By diagonalizing the Hamiltonian in high-dimensional many-body Hilbert space through efficient renormalization and truncation, the DMRG algorithm (in combination with an active-space model)[9,10] is capable of treating many problems that would have been intractable with any other methods, especially the multireference problems with large active spaces (e.g., 100 electrons in 100 active orbitals). The accuracy of DMRG-CASSCF (shortened as DMRG-CAS hereafter) results is close to the (estimated) exact CASSCF results. In addition to the DMRG-CAS approach, dynamic correlation, which is the key to multireference calculations to deliver a qualitative accuracy, can be treated either by the second-order Rayleigh−Schrödinger perturbation theory (DMRG-CASPT2, denoted as DMRG-PT2 hereafter),[11] or by canonical transformation theory (DMRG-CT).[12,13] The capability of combined DMRG-CAS and DMRG-PT2 approaches has been demonstrated on the challenging problem such as electronic states of transition-metal systems.[11]

In such a circumstance, it is very interesting to determine if this combination is suitable for describing a complicated nonadiabatic photochemical reaction. Such an example is the photochromic isomerization of spiropyran (SP) and merocyanine (MC) shown in Scheme 1a. Among the various types of photochemical reaction, the photochromic SP-MC interconversion has attracted considerable attention.[14] Remarkable

Received: August 8, 2013
Published: August 23, 2013

Scheme 1. Schematic Reaction Mechanism for SP Photochromic Ring-Opening Reaction: (a) Genetic Mechanism of SP-MC Photochromic Interconversion; (b) Structure of an Unsubstituted SP with Important Dihedral Angles Defined; (c) Three Important Excited-State C−O/C−N Bond Cleavage Pathways (Blue Background Represents S_1-MEPc, Pink Background Represents S_1-MEPt, and Gray Background Represents S_1-MEP_{CN});[a] and (d) an Alternative H-(C_2) Out-of-Plane (HOOP) Valley near the One-Bond-Flipping (OBF) Path in S_1-MEPt[b]

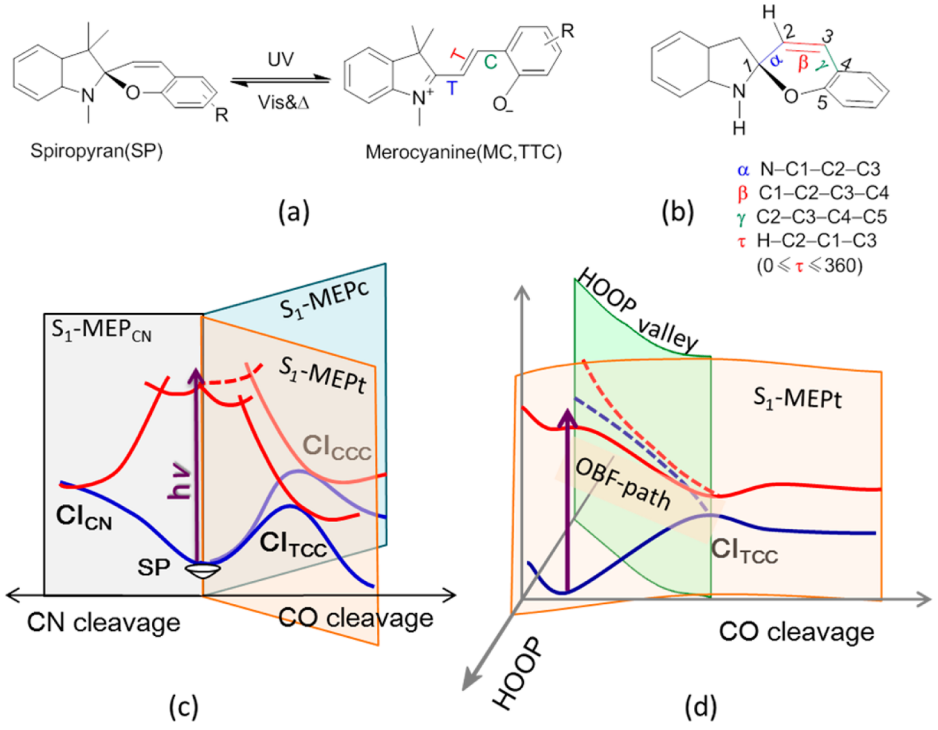

[a]As reported in our previous work.[19] [b]A similar HOOP valley near S_1-MPEc is not shown. Data have been taken from ref 19.

changes in structures and physical/chemical properties between SP and MC make the system an excellent candidate for use in optical molecular devices, such as light-driven molecular switches.[15,16] The reaction channels on the multistate potential energy surfaces (PESs), as well as the overall reaction mechanism, have drawn great attention from theoretical chemists, including us. Several multireference studies have been reported so far. The pioneering CASSCF study by Celani et al.[17] on a benzospiropyran model compound suggested a conical intersection (CI) mechanism occurring from the S_1 state to the S_0 state in the C−O bond cleavage. More-detailed information of the reaction was revealed later by Marta et al.[18] with a simplified SP model at the CASPT2//CASSCF level of theory. They confirmed a deactivation mechanism through S_0/S_1 minimal-energy conical intersection (MECI) and discovered an additional C−N bond cleavage channel. Recently, we explored the multistate reaction of photoinduced ring opening of SP (without simplification on the main framework, as shown in Scheme 1b) at the CASPT2//CASSCF(12e,10o) level.[19] Schemes 1c and 1d illustrate our proposed mechanisms of the excited-state ring opening and possible $S_1 \rightarrow S_0$ transition channels. Our results showed that the MECI(s) on C−O bond breaking channels are less relevant to the internal conversion (IC), because of large dynamic correlations. Instead, alternative valleys on the S_1−PES generated by the active hydrogen-out-of-plane (HOOP) motions, may act as the effective funnels for radiationless $S_1 \rightarrow S_0$ transitions (Figure 1d). The new mechanism, differing from previously proposed ones,[17,18] naturally demands verification by either an experimental study (e.g., time-resolved UV−visible absorption spectroscopic

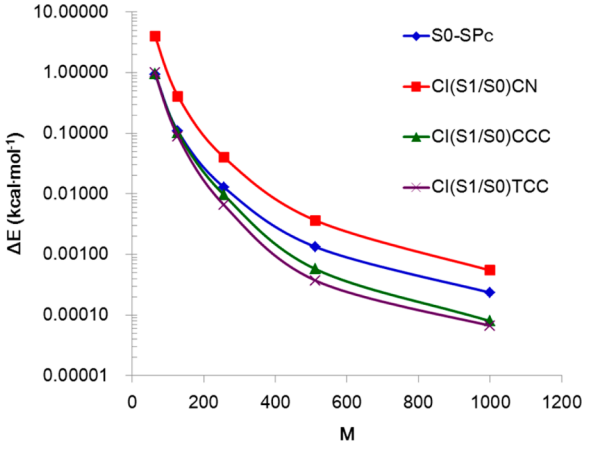

Figure 1. Logarithmic error of the DMRG-CASSCF total energy, with respect to the $M = \infty$ limit, vs$M$. The $M = \infty$ limit energy is obtained by an extrapolation from a linear fit of the energies and discarded weight.[28]

study with isotopic substituents), or a high-level theoretical investigation, for instance, a multireference treatment utilizing a large active space. In the current study, we have carried out the DMRG-CAS and DMRG-PT2 calculations, with a large CAS(22e,20o) active space (see Figure S1 in the Supporting Information), to investigate the photochromic ring-opening step of the unsubstituted SP.

2. COMPUTATIONAL DETAILS

The ab initio DMRG method used here is described in detail in refs 9, 11, and 20. In the DMRG-CAS calculation, the static correlation in an active space is addressed by DMRG. The state-averaged DMRG-CASSCF (SA-CASSCF) WF was adopted, in which the same (averaged) orbitals and renormalized states were used to describe the S_0, S_1, and S_2 states. An active space, CAS(22e,20o), includes all the π/π^* orbitals and σ/σ^* orbitals of both C_1-O and C_1-N bonds. It is a superset of both the CAS(12e,10o) and CAS(12e,10o)$_{CN}$ active spaces in ref 19 and is therefore capable of describing the global PES for both C−O and C−N bond cleavages. The active space is constructed in the same way as that described in ref 20. First, the active orbitals were localized using the Pipek−Mezey localization procedure, and then the localized orbitals were mapped onto a one-dimensional (1D) lattice. (The order of the localized orbitals for the lattice mapping is presented in Figure S1 in the Supporting Information.). For the convenience of discussion, we denoted the CAS(22e,20o) active space as CAS(l), the CAS(12e,10o) active space as CAS(s), and a medium CAS(18e,14o) active space (employed in the vertical excitation energy calculation by conventional CASPT2, shown in Figure S2a in the Supporting Information) as CAS(m). The RASPT2 method[21] was also employed in the vertical excitation energy calculation, in which an active space, RAS(18e,3/10/2o) [denoted as RAS(m), as shown in Figure S2b in the Supporting Information], is constructed.

The molecular structures (including the minima and conical intersections in/between the S_0 and S_1 states, as well as key geometries on the S_1 minimal energy path) were obtained from our previous work;[19] these geometries were optimized at the CASSCF(s)/6-31G(d) level. For SP minima, geometries optimized at the DFT level (i.e., B3LYP structure[22] and CAM-B3LYP structure[19]) were also used in DMRG-CAS and DMRG-PT2 calculations for comparison.

In order to precisely predict the SP geometry and vertical excitation energy, as well to test the capability of DMRG for geometry optimization, we carried out geometry optimization at the DMRG-CAS level, by using an analytical gradient and a state-specific CASSCF (SS-CAS) WF for the S_0 state. The Gaussian 09 program package (Rev. B01)[23] was used as geometry optimizer with a default convergence criterion implemented.

In addition to the DMRG-CAS calculation, the dynamical electron correlations were further evaluated by subsequent DMRG-PT2 calculations.[11] The single-state model (SS-PT2) was used, with a IPEA shift value of 0.25. In both the DMRG-CAS and DMRG-PT2 calculations, the 6-31G(d) basis set[24] (including 277 basis functions) was mainly used. The Dunning triple-ζ basis set, cc-PVTZ[25] (including 721 basis functions) was also employed for some crucial structures for comparison. All conventional CASSCF and CASPT2 calculations were done by using the MOLCAS program (version 7.6).[26,27] All DMRG-CAS and DMRG-PT2 calculations were carried out with our own quantum chemistry package (ORZ).[8,9,11] It should be noted that the present code provides the exact analytical gradient for the single state (SS) DMRG-CAS energy, as well as the approximate analytical gradient for the state-averaged (SA) DMRG-CAS using state-averaged orbitals but for a single-state energy (although we did not use this methodology in the present paper).

3. RESULTS AND DISCUSSIONS

In Section 3.1, we first present the results of our test calculations on the accuracy of DMRG-CAS and DMRG-PT2 WF for the SP ring-opening reaction, with respect to the number of basis states, the number of roots in SA-CASSCF WF, and the number of basis functions. Then, in Section 3.2, we present the electronic excitation properties at the S_0 equilibrium structure, using the geometries optimized at various levels of theories, including the (conventional-)CAS(s) and DMRG-SS-CAS(l) level. In Section 3.3, we show the DMRG-PT2(l)//CAS(s) computed excited-state reaction pathways in detail, compared with conventional PT2(s)//CAS(s) results.

3.1. Tests on the Accuracy of the DMRG-CAS and DMRG-PT2 Results. *Number of Renormalized Basis States (M).* In the DMRG calculations, the number of renormalized basis states (M) included in the calculation plays a key role in determining the accuracy of the DMRG calculation. By increasing M, the DMRG WF may be made arbitrarily more flexible; consequently, the energy may be more accurate. Figure 1 illustrates the error of DMRG-CASSCF total energy (with respect to the $M = \infty$ limit obtained by extrapolation of the energy as a function of discarded weights) versus the number of M. (The total energies for the DMRG-SA3-CAS WFs are summarized in Table S1 in the Supporting Information, along with the total discarded weights, which are the sum of the weights of states truncated in the decimation step and are a measure of the DMRG truncation. The linear extrapolations of the total energy versus the total discarded weight[28] are plotted in Figure S3 in the Supporting Information). As seen in Figure 1, for all four investigated geometries, we already observed fast convergence of DMRG energies with relatively small M. At M = 128, the DMRG WF has converged to an accuracy of better than 0.5 kcal mol^{-1}. These suggest that the HSP molecule is a good candidate for the 1D-lattice DMRG algorithm and also confirms that our mapping of the DMRG orbitals to the 1D lattice (shown in Figure S1 in the Supporting Information) is reasonable.

In addition to the state-averaged energies at the DMRG-SA3-CAS level, the energies of the S_0, S_1, and S_2 states at various structures, relative to the S_0 minimum, at both the DMRG-SA3-CAS and DMRG-SS-PT2 levels (shown in Table S2 in the Supporting Information) also suggest a satisfying accuracy obtained with small M values. Considering the computational costs (see Table S3 in the Supporting Information), in further calculations, we chose a value of M = 128 in the DMRG-CAS and DMRG-PT2 calculations, unless otherwise stated.

Number of Roots in SA-CAS WF. We also evaluated the effects of the number of the roots in state-average DMRG-CAS WFs. With the state-average scheme, one can obtain energies of several states simultaneously (which is generally required for nonadiabatic photochemistry), at the cost of sacrificing the accuracy of individual states. Because of the substantial changes in the geometries and electronic states in all 13 tested structures (see Table S4 in the Supporting Information), we did observe deviations by using different numbers of roots in the DMRG-SAn-CAS (where n = 3, 4, and 6) single-point calculations. The relative energies of S_0, S_1, and S_2 states at various structures show a standard deviation of 1.4 kcal mol^{-1} and the largest deviation of 5.1 kcal mol^{-1}. As a general feature, we also found that, at the S_0 and S_1 minima, the S_1 and S_2 states are close in energy; whereas, at the S_0/S_1 MECIs, the S_2 state is much higher (in energy) than the S_1 (and S_0) state. In all cases,

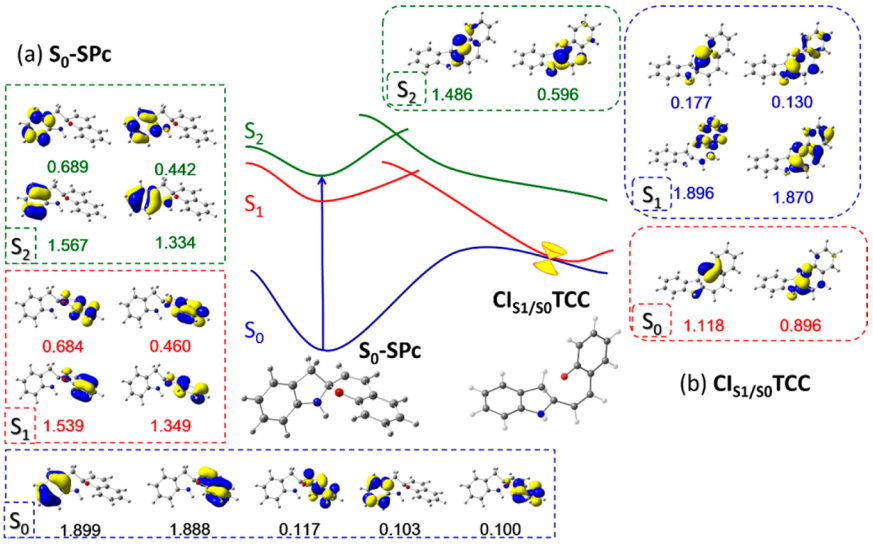

Figure 2. Schematic energy profile along the S_1-MEPt [FC(S_0-SPc) → $CI_{S1/S0}$TCC]. (Here, FC stands for Franck−Condon; for details of the reaction paths, please see ref 19.) The most relevant nature orbitals of the S_0 (in blue box), S_1 (in red box), and S_2 states (in green box) with occupation numbers between 1.8 and 0.2, except for the S_0 state of S_0-SPc (between 1.9 and 0.1) are shown at the geometries of (a) S_0-SPc and (b) $CI_{S1/S0}$TCC reported in ref 19. The NOs and occupation numbers at other important geometries are shown in Figures S4a−d in the Supporting Information.

higher-lying excited states (S_3−S_5) are unnecessary since they are well-separated from lower-lying states. Thus, the SA3-CAS WF, constituted by all necessary number of roots, was chosen in further investigations.

Size of the Basis Set. The third factor affecting the accuracy of the DMRG result is the basis set. A triplet-zeta cc-PVTZ basis set is known to improve the CASSCF and CASPT2 energies (especially the latter). However, by changing the basis set from 6-31G(d) to cc-PVTZ, the number of basis functions are substantially increased from 277 to 721, and the computational time increases in scale by an order of magnitude. For instance, for a parallel DMRG-SS-PT2 job with 16 CPU cores, the total wall clock time increased from ∼7 h [6-31G(d) basis set] to ∼68 h [cc-PVTZ basis set]. (See Table S3 in the Supporting Information.) Note that the increase in computation time in the DMRG calculation itself is comparably small, and it is mainly due to orbital optimization and integral transformation (especially the latter), while such a bottleneck in integral transformation can be avoided using the Resolution-of-Identity (RI) approach that has been recently implemented in ORZ codes. Therefore, cc-PVTZ basis sets were only employed in calculation at some crucial points, and the 6-31G(d) basis set was used for the massive calculations on the reaction paths.

Based on the above-mentioned tests, we set up our computational scheme—that is, a combination of DMRG-SA3-CAS(22e,20o) (M = 128) and DMRG-SS-PT2 (M = 128) with 6-31G(d) basis sets—to explore the reaction path of the HSP ring-opening reaction. We expect that this will provide adequate chemical accuracy that can be used to compare with previous calculations with small active spaces and will provide a more sound basis for understanding the complex reaction mechanism.

3.2. Excited-State Properties at Equilibrium Structure.

For conventional CASSCF and CASPT2 calculation using a truncated active space, the electronic excitation, including both the energy and nature of excitation, is always one of the first concerns. Heavily truncating the active space sometimes misses important electronic excitations and has the risk of formulating the wrong solution (for instance, poor energy or even unphysical excited state). By using an adequate active space size [i.e., the CAS(22e,20o) in this study] beyond the reach of the conventional CASSCF method, we hope that such a risk can be totally avoided, or at least minimized.

Nature of Electronic State at the S_0 Minimum. Figure 2 illustrates the schematic energy profile along one of the C−O bond cleavage processes on the S_1 state, along with the most important natural orbitals (NOs) of S_0 (in blue box), S_1 (in red box), and S_2 states (in green box) and their occupation numbers for S_0-SPc (global ground-state minimum) and $CI_{S1/S0}$TCC (one of the S_1/S_0 MECIs). The details of the excitations are not known, because of the lack of CI coefficients in DMRG-CAS WF. Computing them is not regarded as practical because nontrivial difficulties arise in identifying dominant configurations and interpreting the configurations in localized orbital picture.[4,29] One nonetheless can obviously see the results of the excitation by looking at the NOs and their occupation numbers. At S_0-SPc, electronic transitions from a close-shell singlet (CSS) ground state lead to two low-lying, nearly degenerated excited states. The S_1 state results from the excitations from (and to) active orbitals localized in the chromene moiety, while S_2 is generated from the local excitations in the indoline subunit (for a detailed structure, please see Scheme 1b). These are confirmed by the narrow gap between the S_1 state and the S_2 state at the DMRG-SS-PT2 results shown in Table 1.

Vertical Excitation Energy. Table 1 summarized the DMRG-PT2 computed vertical excitation energies, at optimized geometries at different levels of theory, for the S_0-SPc and S_0-SPt conformers. For comparison, the MS-CASPT2 and MS-RASPT2 energies [based on CAS(s) geometries] with various sizes of active spaces, and the experimentally measured $S_0 \rightarrow S_1$ absorption maxima, are also shown. It is seen from Table 1 that the computed excitation energies at the DMRG-PT2 and conventional CASPT2 level are in consistent with each other, except for the conventional PT2(s)//CAS(s) results show larger errors, because of the small active space. In

dx.doi.org/10.1021/ct400707k | J. Chem. Theory Comput. 2013, 9, 4462−4469

Table 1. Vertical Excitation Energies (eV) at the DMRG-PT2 Level, Along with the Conventional CASPT2/RASPT2 Results on the Basis of Optimized Geometries at Various Level of Theory

PT2//CAS		Vertical Excitation Energy (eV)	
SP	optimal geometry	$S_0 \rightarrow S_1$	$S_0 \rightarrow S_2$
	S_0-SPc		
PT2(s)//[a]	CAS(s)	4.839	4.909
PT2(m)//[b]		4.481	4.735
RASPT2(m)//[c]		4.512	4.881
DMRG-PT2(l)//[d]		4.663	4.806
DMRG-PT2(l)//	DMRG-CAS(l)[e]	4.581	4.758
DMRG-PT2(l)//	CAM-B3LYP	4.630	4.766
DMRG-PT2(l)//	B3LYP	4.547	4.712
	S_0-SPt		
PT2(s)//	CAS(s)	4.805	4.926
PT2(m)//		4.431	4.769
RASPT2(m)//		4.607	4.944
DMRG-PT2(l)//		4.629	4.838
DMRG-PT2(l)//	DMRG-CAS(l)	4.504	4.803
DMRG-PT2(l)//	CAM-B3LYP	4.574	4.824
Exp. Abs		4.161[f]	
		4.203[g]	

[a]MS3-CASPT2(12e,10o)//SA3-CASSCF(12o,10e)/6-31G(d) result, from ref 19. [b]MS3-CASPT2(18e,14o)//SA3-CASSCF(12o,10e)/6-31G(d) results. [c]MS3-RASPT2(S)(18e,3/10/2o)//SA3-CASSCF-(12o,10e)/6-31G(d) results, where "S" stands for the single excitation, and 3/10/2 stands for the number of active orbitals in the RAS1, RAS2, and RAS3 subspace, respectively. [d]DMRG-PT2(M = 256)// SA3-CASSCF(12o,10e)/6-31G(d) results. [e]DMRG-CAS(M = 128)/ 6-31G(d) optimized geometry. [f]Absorption maximum in tetrachloroethene, obtained from ref 30. [g]Absorption maximum in n-pentane, from ref .

addition, the theoretically predicted $S_0 \rightarrow S_1$ absorption energy is consistent with the experimental data, although the former are generally higher than the latter by ∼0.3−0.4 eV (partially due to the absence of zero-point-energy correction and solvent contribution). Furthermore, using the geometries optimized at different levels, the DMRG-PT2 computed vertical excitation energies show some variations (from ∼4.504 eV to 4.663 eV). Therefore, in addition to preciously predicting the single-point energy, refining the ground-state equilibrium geometry at a high level is also desired.

S_0 Minima Optimized with DMRG-CAS WF. We (probably for the first time) carried out geometry optimization of the S_0 minima, using analytic energy gradient for state-specific DMRG-SS-CAS (M = 128) WF with CAS(l) active space. As summarized in Table S5 in the Supporting Information, both S_0-SPc and S_0-SPt conformers [consistent with our previous CAS(s) results][19] are optimized. The DMRG-CAS geometry optimizations (with 16 CPU cores) show great performances (see Figure S5 in the Supporting Information); the geometries for S_0-SPc and S_0-SPt conformers converged smoothly in 10 and 9 optimization cycles, respectively, in a total wall clock time of 58.7 and 57.5 h. The average costs of each optimization step (∼6 h) is almost in the same time scale as that of the conventional CASSCF methods (with much smaller active space). This calculation demonstrated the capability of the DMRG-(CASSCF) as an efficient method in molecular geometry optimization, which opens the possibility to provide reliable photochemical reaction pathways for many larger systems that have been beyond the reach of conventional approaches.

As also seen from Table S5 in the Supporting Information, at the DMRG-CAS level, the optimized S_0-SPc conformer is ∼1.5 kcal mol^{-1} more stable than the DFT and CAS(s) optimized structures, and the optimized S_0-SPt lies ∼1.1 kcal mol^{-1} higher than S_0-SPc. After DMRG-SS-PT2 correction, the order of relative energies changed slightly. Now the global minimum corresponds to the CAM-B3LYP-optimized S_0-SPc, and the S_0-SPt optimized at the same level lies 0.3 kcal mol^{-1} above. The conformers optimized at the DMRG-CAS level are less stable than S_0-SPc (CAM-B3LYP) by ∼0.8 and ∼1.3 kcal mol^{-1} for S_0-SPc and S_0-SPt, respectively. The CAM-B3LYP and DMRG-SS-CAS geometries are lower in energy than others, but the energy differences with different methods are moderate for S_0 minima of SP.

3.3. The S_1-State Ring-Opening Reaction. Now we examine the ring-opening reaction pathways on the S_1 state, namely, the C−O and C−N cleavage processes.

OBF S_1-Minimum Energy Path (MEP). First, we examined the one-bond-flipping (OBF) path that is featured by the cooperation of C−O bond elongation and α bond torsion (for definition of α, see Scheme 1b). Figures 3a−c show the DMRG-PT2(l) energy profiles along the CAS(s)/6-31G(d) optimized S_1-MEPs for S_1-MEPc, S_1-MEPt, and S_1-MEP$_{CN}$, respectively, in comparison with those calculated at the conventional MS-PT2(s) level. As a general trend, we found that for all investigated states, the DMRG-PT2 provides lower relative energies than PT2(s), especially in the initial excitation region (Stage I in Figure 3). Further examination of the energies obtained at various levels of theory, i.e., the DMRG-CAS(l) vs CAS(s) as well as DMRG-PT2(l)-vs DMRG-CAS(l) energies along the S_1-MEPs shown in Figures S6 and S7 in the Supporting Information), suggests that the improvement in energy is most significant when the active space (static correlation) expanded. The dynamic correlation effect for the current DMRG-CAS(l) calculation is less significant than that for the small active space CAS(s) in ref 19, probably because, by increasing the active space, a portion of the dynamic correlation is considered as a nondynamic correlation within the active space. The present result also suggests that DMRG-CAS(l) is an excellent method for treating chemical reactions in excited states.

MECIs on S_1-MEP(OBF). The relative energies of the S_0-state and S_1-state PESs at the S_0/S_1 MECIs is another concern for the SP ring-opening reaction. It is known experimentally that, in *unsubstituted* SP, very efficient IC takes place and more than 90% of the excited molecules go back to ground-state SP.[30,31] However, our previous PT2(s)//CAS(s) results suggested that the wide S_1-S_0 gap caused by large dynamic correlation at the S_0/S_1 MECIs determined by CAS(s), i.e., $CI_{S1/S0}$CCC and $CI_{S1/S0}$TCC (in Figures 3a and 3b), makes IC through this region inefficient.[19] In the DMRG calculations, as mentioned in the previous paragraph, such a large discrepancy in CASPT2 and CASSCF results is not observed. (For detailed comparison, please see Figure S7 in the Supporting Information, where one can see that the DMRG-SS-PT2 energy profiles are in parallel with the DMRG-SA3-CASSCF ones.) As a consequence, at the MECIs, the DMRG-PT2 computed S_1 and S_0 states are close in energy; especially at the $CI_{S1/S0}$CCC, where S_1 and S_0 states are nearly degenerate; therefore, the corresponding probabilities of the radiationless $S_1 \rightarrow S_0$ transitions at $CI_{S1/S0}$CCC and $CI_{S1/S0}$TCC are increased, compared with the PT2(s)

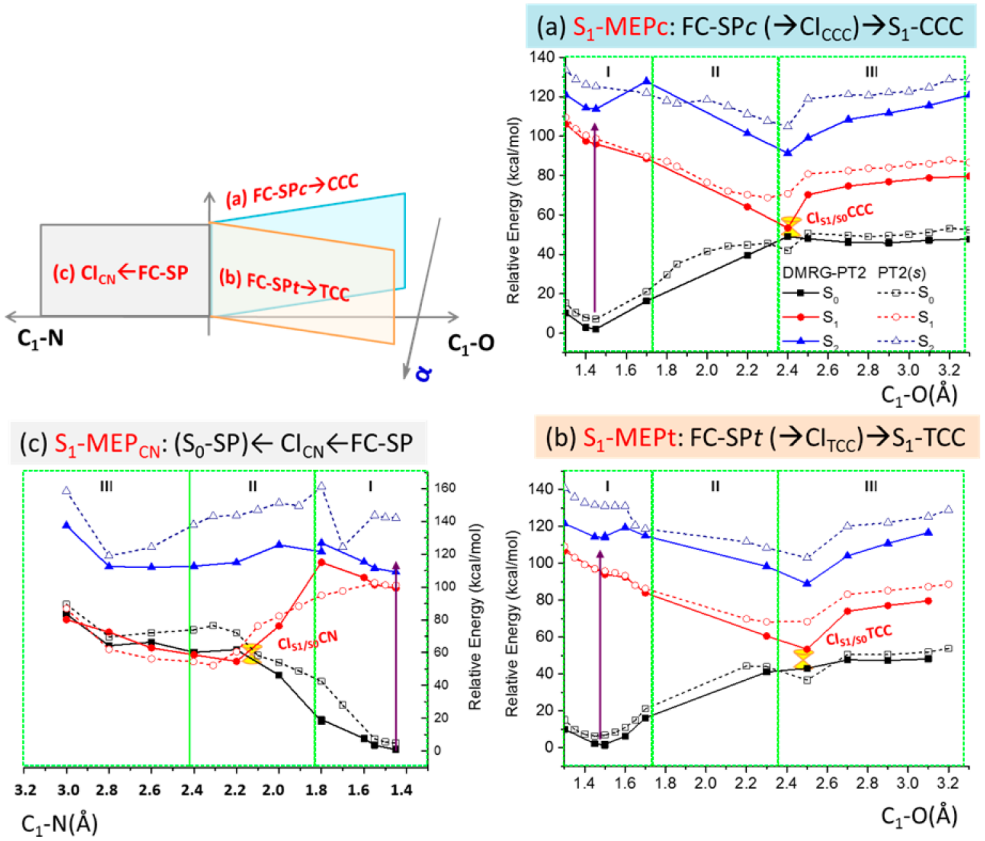

Figure 3. DMRG-PT2(l)//CAS(s) (solid curve and symbols) and PT2(s)//CAS(s) (dashed line with hollow symbols) S_1-MEPs for the ring-opening reaction of (a) S_1-MEPc: FC-SPc → CCC(S_1) path; (b) S_1-MEPt: FC-SP_t →TCC(S_1) path; and (c) S_1-MEP_{CN}: FC-SP → CI_{CN} path. Energies are relative the ground-state energy of the CAS(s)-optimized S_0-SPc. Three reaction stages are divided according to the nature of S_1 state: (I) Initial excitation stage: excitation from S_0-SP to the $(\pi \rightarrow \pi^*)_{SP}$ state, (II) C−O(or C−N) bond-cleavage stage on the $(\pi \rightarrow \sigma^*)$ state, and (III) MC intermediate formation on the $(\pi \rightarrow \pi^*)_{MC}$ state.

predictions. This is the first major difference between the DMRG and conversational results. Another noticeable difference comes from the C−N dissociation MEP (Figure 3c). A barrier is met at a C−N distance of 1.8 Å, when the molecule moves toward the $CI_{S1/S0}$CN, which has been further confirmed by geometry refinements at the DMRG-CAS level with analytical gradient on the S_1 PES. (The DMRG-CAS-optimized S_1-MEP_{CN} is presented in Figure S8 in the Supporting Information.) The ∼10 kcal mol^{-1} barrier makes the C−N bond-cleavage channel less favorable than the C−O dissociation channels.

HOOP Valley near S_1-MEP(OBF). In the previous PT2(s)//CAS(s) study,[19] we have located HOOP valleys near the S_1-MEP(OBF) paths (see bottom figures in Figure 4a and 4b). These HOOP valleys, with similar energies with OBF paths, are expected to be easily accessible with the assistance of the H−(C_2) out-of-plane motion. More interestingly, we found that the S_1 and S_0 states along the HOOP valleys are close in energy with each other; therefore, they may act as alternative funnels for radiationless $S_1 \rightarrow S_0$ transitions.

Figures 4a and 4b (top figures) also show refined energy profiles at the DMRG-PT2(l)//CAS(s) level. Compared with the PT2(s)//CAS(s) results (bottom figures), two evident differences are seen: First, the S_1 state along the HOOP valleys (solid curve and symbols) is in a lower position than that along the OBF paths (dashed curve and hollow symbols), therefore, the HOOP valleys are easier to reach during the C−O cleavage processes. Second, the S_1 and S_0 PES along the DMRG-PT2(l)//CAS(s) MEPs become much closer in energy, in a wide range with a C−O distance of ∼1.7−1.9 Å, i.e. they are nearly degenerate. These will increase the transition probabilities for $S_1 \rightarrow S_0$ nonadiabatic decay. As a consequence of these two changes, the HOOP valleys, as suggested by DMRG-PT2 calculations, are expected to play (more) important roles in the internal conversion process.

In summary, the DMRG-PT2(l)//CAS(s) results show good consistency with the PT2(s) ones; therefore, the reaction mechanism discovered in our previous study[19] is confirmed by a higher-level calculation with substantially larger active space. More specifically, DMRG results, compared with the previous results with small active space, suggest more important role of the HOOP valleys near the C−O S_1-MEPs and the MECI along the S_1-MEPs in the radiationless $S_1 \rightarrow S_0$ transitions, while the transition along the C−N bond dissociation path is less favorable, because of a barrier on the S_1-MEP_{CN}.

4. CONCLUSIONS

The photochromic ring-opening reaction of spiropyran has been revisited at the multireference DMRG-CASSCF and DMRG-CASPT2 levels. A substantially larger active space (labeled l) than before, (22e,20o), including all π/π^* orbital and C−O and C−N σ/σ^* orbital, is used. Some conclusions are drawn:

(1) First of all, our DMRG-CASSCF calculations suggest that the spiropyran molecule is suited to the one-dimensional (1-D) algorithm in the DMRG approach,

dx.doi.org/10.1021/ct400707k | J. Chem. Theory Comput. 2013, 9, 4462−4469

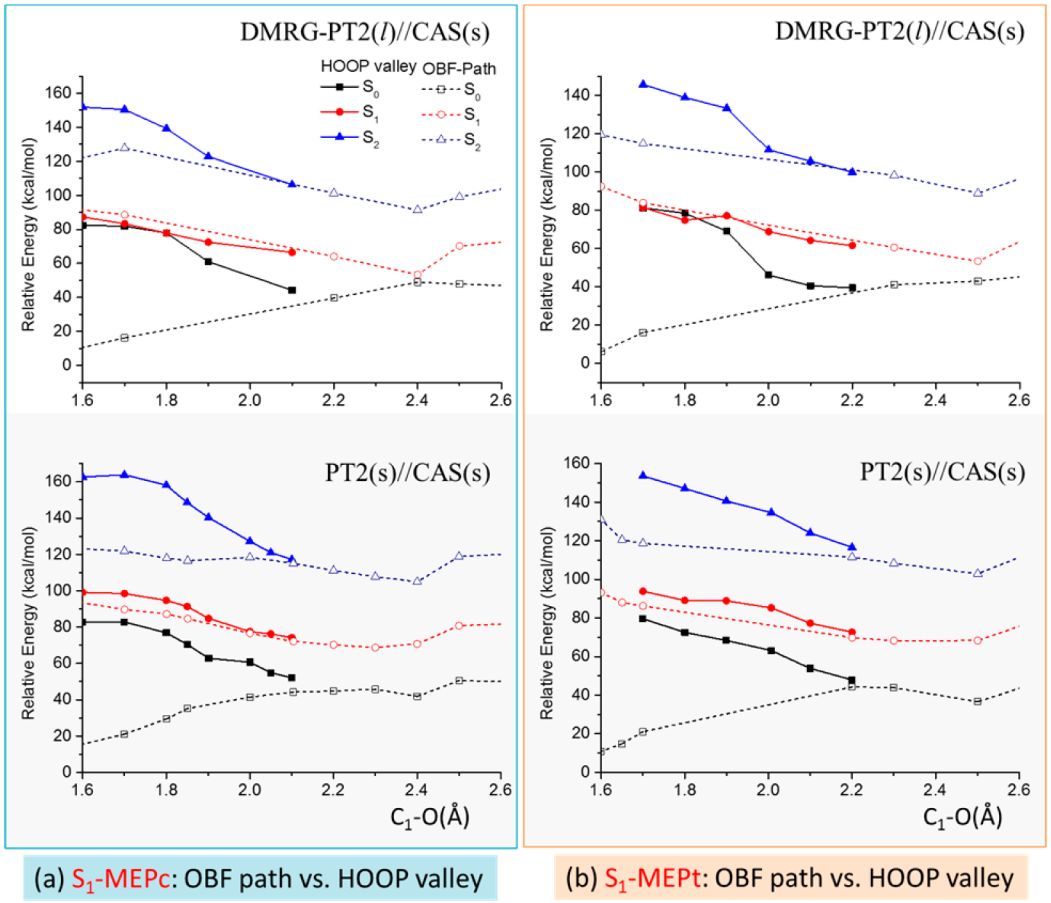

Figure 4. S_1-MEP(OBF) paths and S_1−HOOP-valley for (a) SP → CCC and (b) SP → TCC. Top panel: The DMRG-PT2(l)//CAS(s). Bottom panel: PT2(s)//CAS(s) for HOOP-valley (solid curve and symbols) and OBF-path (dashed line with hollow symbols).

and therefore, accurate energy can be obtained with a relatively smaller number of renormalized states (M). At M = 128, the DMRG WF has converged to an accuracy of better than 0.5 kcal mol^{-1}.

(2) The nature and vertical excitation energies of the excited (S_1 and S_2) states are investigated at the DMRG-CASPT2(l) level. Both of them feature local excitation, within the chromene (S_1) and indoline (S_2) subunit. (The charge-transfer states are higher in energy.) The vertical excitation energies obtained at the DMRG-CASPT2(l) level are consistent with those by conventional CAS(or RAS)PT2 with a medium active space.

(3) We have demonstrated the capability of the DMRG-SS-CASSCF method in optimization of molecular geometry, using a large active space and an analytical gradient. The computation costs are comparable to that of the conventional CASSCF geometry optimization with a much smaller active space.

(4) Finally, the DMRG-PT2(l)//CAS(s) computed S_1-MEP for the C−O and C−N bond cleavage show good agreement with our previous calculations with the PT2(s)//CAS(s) approach.[19] The roles of the HOOP valleys in the $S_1 \rightarrow S_0$ nonadiabatic decay have been confirmed.

■ ASSOCIATED CONTENT

Supporting Information

Figures S1−S8, Tables S1−S5, and Cartesian coordinates for the key structures. This material is available free of charge via the Internet at http://pubs.acs.org.

■ AUTHOR INFORMATION

Corresponding Author

*E-mail: morokuma@fukui.kyoto-u.ac.jp.

Notes

The authors declare no competing financial interest.

■ ACKNOWLEDGMENTS

Authors are grateful to Drs. Lung Wa Chung, Miho Hatanaka, Lina Ding, Travis Harris for fruitful discussions and generous help. This work is in part supported by Japan Science and Technology Agency (JST) with a Core Research for Evolutional Science and Technology (CREST) grant in the Area of High Performance Computing for Multiscale and Multiphysics Phenomena and in part by grants from Japan Society for the Promotion of Science (Grants-in-Aid for Scientific Research <KAKENHI> No. 24245005 at Kyoto University as well as No. 25410030 and No. 25288013 at Institute for Molecular Science). A generous support of computational resources at Research Center of Computer Science (RCCS) at the Institute for Molecular Science (IMS) is acknowledged.

REFERENCES

(1) Roos, B. O. In *Advances in Chemical Physics*; John Wiley & Sons: New York, 1987; Vol. *69*, pp 399−445.
(2) Schollwöck, U. *Rev. Mod. Phys.* **2005**, *77*.
(3) Mitrushenkov, A. O.; Fano, G.; Ortolani, F.; Linguerri, R.; Palmieri, P. *J. Chem. Phys.* **2001**, *115*, 6815.
(4) Chan, G. K.-L.; Head-Gordon, M. *J. Chem. Phys.* **2002**, *116*, 4462.
(5) Legeza, Ö.; Fáth, G. *Phys. Rev. B* **1996**, *53*, 14349−14358.
(6) Marti, K. H.; Ondík, I. M.; Moritz, G.; Reiher, M. *J. Chem. Phys.* **2008**, *128*, 014104.
(7) Zgid, D.; Nooijen, M. *J. Chem. Phys.* **2008**, *128*, 014107.
(8) Kurashige, Y.; Yanai, T. *J. Chem. Phys.* **2009**, *130*, 234114.
(9) Ghosh, D.; Hachmann, J.; Yanai, T.; Chan, G. K.-L. *J. Chem. Phys.* **2008**, *128*, 144117.
(10) Zgid, D.; Nooijen, M. *J. Chem. Phys.* **2008**, *128*, 144115.
(11) Kurashige, Y.; Yanai, T. *J. Chem. Phys.* **2011**, *135*, 094104.
(12) Neuscamman, E.; Yanai, T.; Chan, G. K.-L. *J. Chem. Phys.* **2010**, *132*, 024106.
(13) Yanai, T.; Kurashige, Y.; Neuscamman, E.; Chan, G. K.-L. *J. Chem. Phys.* **2010**, *132*, 024105.
(14) Tamai, N.; Miyasaka, H. *Chem. Rev.* **2000**, *100*, 1875−1890.
(15) Saha, S.; Stoddart, J. F. *Chem. Soc. Rev.* **2007**, *36*, 77−92.
(16) Feringa, B. L.; Van Delden, R. A.; Koumura, N.; Geertsema, E. M. *Chem. Rev.* **2000**, *100*, 1789−1816.
(17) Celani, P.; Bernardi, F.; Olivucci, M.; Robb, M. A. *J. Am. Chem. Soc.* **1997**, *119*, 10815−10820.
(18) Sanchez-Lozano, M.; Estévez, C. M.; Hermida-Ramón, J.; Serrano-Andres, L. *J. Phys. Chem.* **2011**, *115*, 9128−9138.
(19) Liu, F.; Morokuma, K. *J. Am. Chem. Soc.* **2013**, *135*, 10693−10702.
(20) Kurashige, Y.; Chan, G. K.; Yanai, T. *Nat. Chem.* **2013**, 1−7.
(21) Malmqvist, P. A.; Pierloot, K.; Shahi, A. R. M.; Cramer, C. J.; Gagliardi, L. *J. Chem. Phys.* **2008**, *128*, 204109.
(22) Sheng, Y.; Leszczynski, J.; Garcia, A. A.; Rosario, R.; Gust, D.; Springer, J. *J. Phys. Chem. B* **2004**, *108*, 16233−16243.
(23) Frisch, M. J.; Trucks, G. W.; Schlegel, H. B.; Scuseria, G. E.; Robb, M. A.; Cheeseman, J. R.; Scalmani, G.; Barone, V.; Mennucci, B.; Petersson, G. A.; Nakatsuji, H.; Caricato, M.; Li, X.; Hratchian, H. P.; Izmaylov, A. F.; Bloino, J.; Zheng, G.; Sonnenberg, J. L.; Hada, M.; Ehara, M.; Toyota, K.; Fukuda, R.; Hasegawa, J.; Ishida, M.; Nakajima, T.; Honda, Y.; Kitao, O.; Nakai, H.; Vreven, T.; Montgomery, J. A.; Peralta, J. E.; Ogliaro, F.; Bearpark, M.; Heyd, J. J.; Brothers, E.; Kudin, K. N.; Staroverov, V. N.; Kobayashi, R.; Normand, J.; Raghavachari, K.; Rendell, A.; Burant, J. C.; Iyengar, S. S.; Tomasi, J.; Cossi, M.; Rega, N.; Millam, J. M.; Klene, M.; Knox, J. E.; Cross, J. B.; Bakken, V.; Adamo, C.; Jaramillo, J.; Gomperts, R.; Stratmann, R. E.; Yazyev, O.; Austin, A. J.; Cammi, R.; Pomelli, C.; Ochterski, J. W.; Martin, R. L.; Morokuma, K.; Zakrzewski, V. G.; Voth, G. A.; Salvador, P.; Dannenberg, J. J.; Dapprich, S.; Daniels, A. D.; Farkas, Ö.; Foresman, J. B.; Ortiz, J. V.; Cioslowski, J.; Fox, D. J. *Gaussian 09, Revision B.01*; Gaussian, Inc.: Wallingford, CT, 2009.
(24) Ditchfield, R. *J. Chem. Phys.* **1971**, *54*, 724.
(25) Woon, D. E.; Dunning, T. H. *J. Chem. Phys.* **1995**, *103*, 4572.
(26) Karlström, G.; Lindh, R.; Malmqvist, P.-Å.; Roos, B. O.; Ryde, U.; Veryazov, V.; Widmark, P.-O.; Cossi, M.; Schimmelpfennig, B.; Neogrady, P.; Seijo, L. *Comput. Mater. Sci.* **2003**, *28*, 222−239.
(27) Lindh, R. *J. Comput. Chem.* **2010**, *31*, 224−247.
(28) Chan, G. K.-L.; Head-Gordon, M. *J. Chem. Phys.* **2003**, *118*, 8551.
(29) Moritz, G.; Reiher, M. *J. Chem. Phys.* **2007**, *126*, 244109.
(30) Rini, M.; Holm, A.-K.; Nibbering, E. T. J.; Fidder, H. *J. Am. Chem. Soc.* **2003**, *125*, 3028−34.
(31) Ernsting, N. P.; Arthen-Engeland, T. *J. Phys. Chem.* **1991**, *95*, 5502−5509.